J. Phys. Chem. Solids Vol. 50, No. 7, pp 743–751, 1989
Printed in Great Britain

0022-3697/89 $3.00 + 0.00

CALORIMETRIC STUDY OF PHASE TRANSITIONS IN AMMONIUM HYDROGEN OXALATE HEMIHYDRATE AND ITS DEUTERATED COMPOUND†

MARI FUKAI, TAKASUKE MATSUO and HIROSHI SUGA
Department of Chemistry and Chemical Thermodynamics Laboratory, Faculty of Science, Osaka University, Toyonaka, Osaka 560, Japan

(*Received* 7 *November* 1988; *accepted* 1 *February* 1989)

Abstract—The molar heat capacities of ammonium hydrogen oxalate hemihydrate and its fully-deuterated compound were measured from 13 to 300 K. A higher-order phase transition was found in each compound. The temperatures and molar entropies of transition are 145.4 K (6.01 J K^{-1} mol^{-1}) and 160.1 K (8.23 J K^{-1} mol^{-1}) in the protonated and deuterated compounds, respectively, where the mole refers to $(NH_4HC_2O_4)_2 \cdot H_2O$ or $(ND_4DC_2O_4)_2 \cdot D_2O$. The entropies of the transitions indicate that they are order–disorder transitions, probably related to the ordering of one of the ammonium ions. The pressure coefficient of the transition temperature was calculated by the Ehrenfest relation and the available data of the thermal expansivity of the hydrogenous compound: -2.0×10^7 Pa K^{-1} in good agreement with a reported value -1.9×10^7 Pa K^{-1} based on a high pressure experiment.

Keywords: Phase transition, heat capacity, entropy of transition, ammonium hydrogen oxalate hemihydrate, ammonium hydrogen oxalate hemihydrate $-d_6$, order–disorder transition, soft mode.

1. INTRODUCTION

Ammonium hydrogen oxalate hemihydrate $(NH_4HC_2O_4)_2 \cdot H_2O$ (hereafter called AHO) belongs to the orthorhombic space group $Pmnb(D_{2h}^{16})$ at room temperature [1]. In this crystal the C_2O_4 group has nearly planar configuration, and the hydrogen oxalate ions are linked by short hydrogen bonds (0.2561 nm) along the b-axis to form infinite chains. These chains are connected along the a-axis by weaker hydrogen bonds via H_2O molecules and by ionic interactions via NH_4^+ ions. The high anisotropies of the elastic constants [2] and the thermal expansion [3] were related to this bond scheme. Both the H_2O molecules and the NH_4^+ ions lie on a mirror plane. For NH_4^+ ions, there are two symmetrically independent families. It has been suggested from X-ray studies [1] that one of the NH_4^+ families has a statistical character in which each NH_4^+ ion belonging to that family can take one of the two orientations symmetric with respect to the mirror plane. Measurement of the temperature dependence of the lattice parameters revealed that AHO undergoes, at $T_{trs} = 145.6$ K, a second-order ferroelastic phase transition, which leads to the monoclinic space group $P2_1/n$ (C_{2h}^5) [4]. This phase transition is accompanied by softening of an elastic constant C_{55} whose behavior above and below T_{trs} was discussed in terms of the Landau theory that takes into account the coupling between a microscopic order parameter Q, the xz shear deformation e_5 and the principal deformations $e_i (i = 1, 2, 3)$ [5]. In a Raman scattering experiment [6], the microscopic parameter Q responsible for the transition was identified with the ordering of one family of NH_4^+ ions. Strong fluctuation of Q associated with the ordering induced a central peak in the Raman scattering.

Complete softening of an acoustic vibration is, however, often associated with displacive transitions. Since clear distinction between order–disorder and displacive transitions can be made by an experimental determination of the transition entropy, we measured the heat capacity of AHO in order to investigate the thermal anomaly due to the phase transition. For this compound, a detailed set of thermal expansivity and elastic tensor components have been determined as functions of temperature. Thermal expansivities, substituted into the Ehrenfest relationship together with the experimental heat capacity discontinuity at the transition give the magnitude of dP/dT, for which an experimental value was reported very recently [7]. This gives a numerical check of the consistency of the existing experimental data.

We also measured the heat capacity of $(ND_4DC_2O_4)_2 \cdot D_2O$ (hereafter designated as ADO) in order to investigate the isotope effect on the transition.

2. EXPERIMENTAL

AHO was prepared from an equimolar aqueous solution of oxalic acid and ammonium oxalate and recrystallized from a hot aqueous solution. The elemental analysis gave: C, 20.76% (calc. 20.70%); H, 5.16% (5.21%); N, 12.02% (12.07%). ADO was

---

† Contribution No. 158 from the Chemical Thermodynamics Laboratory.

obtained by repeated recrystallization of AHO from D_2O. At the end of the fourth recrystallization, the proton content of recovered D_2O solvent was determined by NMR spectroscopy in order to estimate the deuteration level of the sample. Potassium benzoate whose aromatic protons do not exchange with the aqueous hydrogen (or deuterium) was dissolved in the recovered D_2O sample as an internal standard for the intensity measurement. The deuteration ratio thus determined was 99.8%. The crystal was assumed to have the same deuteration level as the recrystallization solvent.

The heat capacity measurements were made with an automatic adiabatic calorimeter [8, 9] between 13 and 300 K. The mass of the calorimetric sample was 15.5859 g for AHO and 3.7925 g for ADO. Different cells were used for the normal and deuterated samples. The infrared spectra of the two compounds were measured in the 4000–400 cm^{-1} wavenumber range at liquid nitrogen temperature.

3. RESULTS AND DISCUSSION

3.1. *Experimental results*

There are 81 vibrational degrees of freedom in $(NH_4HC_2O_4)_2\cdot H_2O$ (AHO) or $(ND_4DC_2O_4)_2\cdot D_2O$ (ADO). The observed absorption bands were assigned by comparison with the well-documented spectra of $NaHC_2O_4\cdot H_2O$ and $NaDC_2O_4\cdot D_2O$ taken at −180°C [10]. The assignments are given in Table 1. The values in parentheses were not observed in AHO or ADO but reported for the corresponding sodium salts [10]. All the wavenumbers in Table 1 were used in the normal heat capacity calculation described later.

The experimental molar heat capacities of AHO and ADO are tabulated in temperature-increasing order in Tables 2 and 3, respectively, and plotted in Fig. 1. The dotted curves in the figure represent the normal heat capacities determined as described below. Thermal anomalies due to the higher-order

Table 1. Observed wavenumbers (cm^{-1}) of $(NH_4HC_2O_4)_2$ H_2O(AHO) and $(ND_4DC_2O_4)_2\cdot D_2O$(ADO), and their assignments. Infrared and Raman data taken at liquid nitrogen temperature

	Weight	AHO	ADO		Weight	AHO	ADO
$2NH_4^+, 2ND_4^+$				2H, 2D			
ν_1	2	3020	2193	ν(OH, OD)	2	(1880)†	1329‡
ν_2	4	1702	1214	δ(OH, OD)	2	1454	1084
ν_3	6	3101	2380	γ(OH, OD)	2	(1042)	754
ν_4	6	1395	1078, 1059, 1053§				
T	6	?	?				
R	6	?	?				
$2C_2O_4^{2-}$				H_2O, D_2O			
ν(C=O)	2	1721	1729	ν_1	1	3335	2448
ν_s(COO$^-$)	2	1395	1440	ν_2	1	1622	1214
ν_a(COO$^-$)	2	1622	1638	ν_3	1	3335	2509
ν(C–O)	2	1222	1271	T	1	(287)	(281)
ν(C–C)	2	881	885	T	1	(197)	(192)
δ(COO$^-$)	2	725	676	T	1	(178)	(172)
δ(COO$^-$)	2	503	493	R	1	(685)	532
ρ(COO$^-$)	2	(608)	563	R	1	(608)	459
ρ(COO$^-$)	2	464	459	R	1	587	433
wag(COO$^-$)	2	(328)	(325)				
wag(COO$^-$)	2	(234)	(226)				
twist(COO$^-$)	2	?	?				
T	6	?	?				
R	2	(80)	(80)¶				
R	4	?	?				

† Values in parentheses indicate citation from Table 1 in Ref. 10 (see the text in detail).

‡ $\nu(OD) = \nu(OH)/\sqrt{2}$.

§ A weight of two was assigned to each of the three wavenumbers.

¶ Value in $NaHC_2O_4\cdot H_2O$.

Table 2. Heat capacity of $(NH_4HC_2O_4)_2 \cdot H_2O$

T/K	C_p/$J \cdot K^{-1} \cdot mol^{-1}$	T/K	C_p/$J \cdot K^{-1} \cdot mol^{-1}$	T/K	C_p/$J \cdot K^{-1} \cdot mol^{-1}$	T/K	C_p/$J \cdot K^{-1} \cdot mol^{-1}$
13.35	3.466	88.16	140.4	143.81	232.0	162.00	221.8
14.57	4.560	90.47	144.0	144.08	232.5	164.03	223.6
15.31	5.304	92.72	147.6	144.34	233.2	166.05	225.5
16.03	6.094	94.92	150.9	144.60	234.1	168.06	227.3
16.72	6.910	97.08	154.3	144.94	234.8	170.05	229.1
17.40	7.740	99.19	157.6	145.12	235.3	172.03	230.9
18.14	8.778	101.27	160.5	145.31	235.5	174.00	232.7
19.00	9.988	103.30	163.6	145.38	235.9	175.96	234.5
19.83	11.28	105.31	166.6	145.41	235.9	177.91	236.2
20.59	12.50	107.28	169.7	145.51	235.7	179.85	238.0
21.31	13.66	109.22	172.6	145.60	235.4	181.78	239.7
22.02	14.86	111.13	175.5	145.64	235.4	183.70	241.4
22.72	16.08	113.01	178.4	145.70	234.8	185.61	243.1
23.38	17.28	114.87	181.2	145.80	234.0	187.50	244.7
24.03	18.51	116.71	184.1	145.90	233.0	189.39	246.3
24.92	20.19	118.52	186.8	145.90	232.5	191.27	248.0
26.01	22.33	120.31	189.7	146.00	230.4	193.14	249.6
27.09	24.48	122.07	192.4	146.10	223.4	195.00	251.2
28.13	26.59	123.82	195.2	146.17	218.1	196.85	252.8
29.10	28.58	125.55	198.0	146.20	214.3	198.69	254.4
30.05	30.61	127.26	200.7	146.30	210.3	200.52	256.0
31.13	32.89	128.24	202.3	146.41	209.7	202.35	257.5
32.42	35.71	128.95	203.5	146.51	209.3	204.16	259.0
33.73	38.54	129.41	204.2	146.62	208.8	205.97	260.6
34.94	41.22	130.62	206.3	146.72	208.5	207.77	262.1
36.11	43.78	131.23	207.3	146.83	208.3	209.57	263.5
36.17	43.91	132.28	209.1	146.93	208.3	211.48	265.1
37.24	46.23	133.72	211.6	147.00	208.6	213.52	266.9
37.29	46.35	133.92	212.0	147.04	208.6	215.55	268.6
38.31	48.56	135.54	215.1	147.27	208.4	217.58	270.2
38.36	48.68	136.16	216.0	147.49	208.8	219.96	272.2
39.36	50.83	137.10	217.7	147.55	208.9	222.69	274.4
39.40	50.94	137.15	217.9	147.81	208.8	225.41	276.6
40.38	53.05	137.26	217.9	148.08	209.1	228.11	278.9
40.42	53.16	137.42	218.2	148.09	209.2	230.80	281.2
41.39	55.23	137.63	218.6	148.36	209.3	233.47	283.2
42.30	57.21	137.91	219.1	148.63	209.7	236.13	285.3
43.19	59.10	138.18	219.8	148.92	209.9	238.77	287.5
44.05	60.93	138.46	220.3	149.19	210.1	241.40	289.6
45.04	63.01	138.51	220.5	149.47	210.3	244.02	291.8
46.15	65.37	138.73	220.9	149.68	210.5	246.62	293.7
47.28	67.77	138.74	221.0	149.74	210.5	249.21	295.7
48.43	70.09	139.00	221.3	149.80	210.6	251.79	297.6
49.55	72.40	139.27	221.9	150.01	210.7	254.35	299.7
50.64	74.68	139.54	222.4	150.29	211.0	256.90	301.7
52.21	77.84	139.81	223.2	150.56	211.3	259.44	303.7
54.21	81.79	140.08	223.5	150.84	211.7	261.97	305.7
56.12	85.54	140.31	224.1	151.11	211.8	264.48	307.7
57.95	89.08	140.35	224.2	151.38	212.0	266.99	309.7
58.62	90.29	140.62	224.8	151.65	212.1	269.48	312.0
59.79	92.52	140.79	225.1	151.93	212.4	276.80	317.6
61.79	96.16	140.89	225.4	152.10	212.6	279.25	319.5
64.75	101.5	141.16	225.9	152.47	212.9	281.68	321.3
67.55	106.5	141.43	226.4	152.74	213.1	284.11	323.2
70.21	111.1	141.69	226.9	153.01	213.5	286.53	325.1
72.74	115.4	141.87	227.4	153.28	213.7	288.94	327.0
75.18	119.5	141.96	227.7	153.56	213.8	291.33	328.8
77.54	123.4	142.23	228.3	153.83	214.1	293.72	330.5
79.81	127.1	142.49	228.7	154.10	214.6	296.10	332.3
80.84	128.7	142.76	229.4	154.37	214.7	298.47	334.0
82.02	130.7	143.02	229.9	154.64	215.1	300.83	335.8
83.35	132.7	143.29	230.9	155.81	216.1		
84.17	134.1	143.41	231.1	157.89	217.9		
85.79	136.7	143.55	231.5	159.95	219.9		

phase transitions were observed at 145.4 and 160.1 K in AHO and ADO, respectively. These transition temperatures are in good agreement with those found by X-ray [4] (T_{trs} = 145.6 K in AHO) and neutron experiments [7] (T_{trs} = 160 K in ADO).

We repeated the measurement several times over the transition regions to check the reproducibility of the data. For AHO, the data in four series agreed very well with each other, and all the experimental data are given in Table 2. For ADO, however, the data of the different series deviated systematically from each other by 0.25–0.4% apparently depending on the starting temperature of measurement to which the sample was cooled down from above the transition point, as shown in Fig. 2. The largest deviation ($\simeq$0.4% of the C_p) resulted when the measurement was started at *ca* 12 K below T_{trs}. This hysteretic behavior may be connected with the spontaneous

Table 3. Heat capacity of $(ND_4DC_2O_4)_2 \cdot D_2O$

T/K	C_p/J·K^{-1}·mol^{-1}	T/K	C_p/J·K^{-1}·mol^{-1}	T/K	C_p/J·K^{-1}·mol^{-1}	T/K	C_p/J·K^{-1}·mol^{-1}
13.95	4.561	80.75	138.3	153.09	255.8	183.50	260.2
14.83	5.510	81.04	138.7	153.38	256.2	186.57	263.0
15.71	6.514	82.63	141.5	153.67	257.0	189.61	265.8
16.59	7.615	82.84	141.7	153.96	257.7	192.63	268.4
17.46	8.817	84.60	144.8	154.24	258.3	195.63	271.2
18.34	10.14	86.33	147.6	154.27 †	259.3	198.61	273.9
19.20	11.50	86.40	148.0	154.53	258.9	201.56	276.5
20.04	12.95	88.02	150.4	154.82	259.4	204.50	279.2
20.86	14.37	88.43	151.3	155.11	260.3	207.42	281.6
21.68	15.82	89.67	153.4	155.41	260.4	210.32	284.2
22.50	17.35	90.40	154.4	155.70	261.6	213.21	286.8
23.30	18.88	92.34	157.8	155.88 †	262.5	216.07	289.4
24.11	20.47	94.24	160.8	155.99	262.0	218.92	291.8
24.93	22.14	96.26	164.3	156.29	262.5	221.76	294.2
25.72	23.79	98.39	167.6	156.58	263.2	224.66	296.8
26.52	25.44	100.48	170.9	156.88	263.7	227.63	299.6
27.67	27.92	102.53	174.2	157.17	264.6	230.58	302.5
29.08	30.99	104.55	177.4	157.47	264.6	233.52	304.4
30.40	33.91	106.61	180.7	157.48 †	265.8	236.43	307.1
31.70	36.83	108.73	184.0	157.76	265.6	239.33	309.8
32.98	39.76	110.82	187.2	158.06	265.9	242.22	312.4
34.34	42.88	112.87	190.4	158.36	266.8	245.08	314.6
35.77	46.18	114.90	193.5	158.66	267.0	247.94	317.0
37.15	49.31	116.89	196.7	158.95	268.0	250.78	319.4
38.52	52.44	118.86	199.7	159.06 †	268.8	253.60	321.9
39.97	55.69	120.81	202.7	159.25	268.3	256.41	324.4
41.44	59.05	122.74	205.7	159.55	269.0	258.11	326.2
43.04	62.71	124.64	208.7	159.84	269.2	259.20	326.7
44.71	66.42	126.52	211.6	160.14	269.2	260.17	327.9
46.29	69.98	128.38	214.6	160.43	268.8	261.98	329.1
47.93	73.70	130.22	217.4	160.73	267.5	262.23	329.6
49.64	77.39	132.04	220.3	161.02	263.2	264.74	331.4
51.26	80.89	133.85	223.3	161.32	253.8	266.31	333.2
51.53	81.46	135.63	226.1	161.63	246.3	267.49	333.9
52.87	84.46	137.40	228.9	161.94	244.7	268.34	334.9
53.36	85.38	139.16	231.9	162.24	244.0	270.23	336.4
54.46	87.79	140.90	234.8	162.55	243.4	270.36	336.6
54.79	88.70	142.62	237.6	162.86	243.3	272.37	338.2
56.00	90.99	144.32	240.7	163.17	243.3	274.38	340.1
56.17	91.48	146.02	243.7	163.47	243.4	276.38	341.3
57.51	94.11	147.69	246.7	163.78	243.4	278.38	343.3
57.53	94.26	148.97	248.0	164.09	243.7	280.37	345.0
58.80	96.64	149.27	248.7	164.40	243.9	280.91	345.4
59.05	97.39	149.36 †	249.8	164.70	243.8	282.35	346.5
60.05	99.35	149.57	249.3	165.01	244.0	283.58	347.8
60.53	100.3	149.86	250.6	165.53	244.7	284.32	348.1
61.32	102.0	150.16	250.2	167.15	245.8	286.22	350.1
62.61	104.4	150.45	250.9	168.78	247.0	288.25	351.8
63.87	107.0	150.75	251.5	170.39	248.5	288.86	352.5
65.09	109.4	151.01 †	252.8	170.80	248.6	290.20	353.6
66.29	111.6	151.04	252.1	172.00	249.9	291.48	354.3
67.45	113.8	151.33	252.4	173.60	251.2	292.15	354.9
69.13	117.1	151.63	253.1	175.19	252.7	294.09	356.5
71.28	121.0	151.92	253.7	176.12	253.3	294.09	356.4
73.35	124.9	152.21	254.2	176.78	254.0	296.03	358.0
75.35	128.6	152.50	254.8	178.25	255.4	296.69	358.8
77.30	131.9	152.65 †	256.0	178.50	255.7	299.27	361.0
79.19	135.5	152.79	255.3	180.63	257.7		

† In the range 148.97–165.01 K, data with a dagger represent those of series 1 (cooled down to 79.79 K), and data without a dagger those of series 2 (cooled down to 148.82 K).

strain associated with the ferroelastic transition. However, definite correlation between the temperature cycling and the heat capacity change could not be established because of the small magnitude of the effect.

Table 3 only contains representative data, because the entire collection of the data is too large to be useful. The tabulated values were used in the calculation of the excess heat capacity and the thermodynamic functions.

3.2. *Determination of the excess heat capacity and transition entropy*

In order to derive the enthalpy and entropy of the transition, the base line of the heat capacity was determined by interpolation of the normal heat ca-

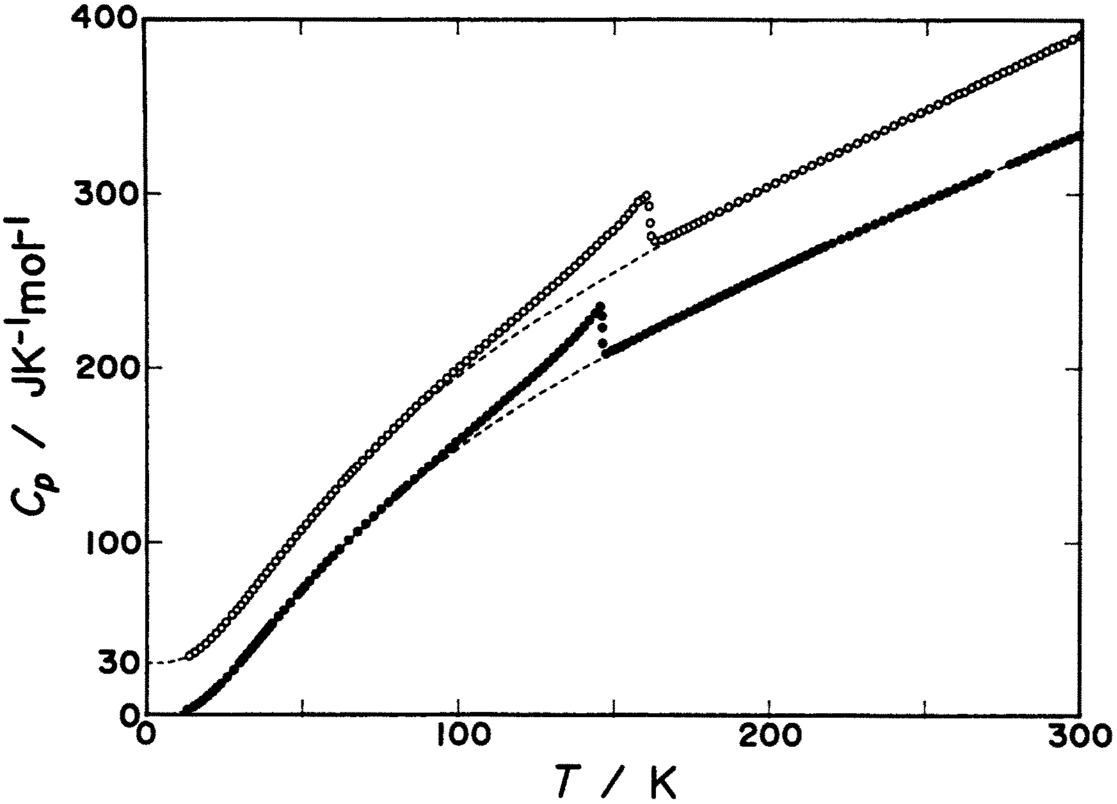

Fig. 1. Heat capacities of $(NH_4HC_2O_4)_2 \cdot H_2O$ and $(ND_4DC_2O_4)_2 \cdot D_2O$. (●), $(NH_4HC_2O_4)_2 \cdot H_2O$ (AHO); (○), $(ND_4DC_2O_4)_2 \cdot D_2O$ (ADO). The curve for ADO is shifted upwards by 30 J K^{-1} mol^{-1} for the sake of clarity.

pacity into the transition region. We adopted a combination of the Debye and Einstein functions for the interpolation function. The characteristic temperatures were determined from the vibrational analyses and by fitting the model function to the experimental data which we regarded free from anomalous contribution. The temperature range and the number of points used for the fitting are given in Table 4. We deemed the transition region as extending between 40 and 175 K, and 67 and 207 K for AHO and ADO, respectively (see Table 4).

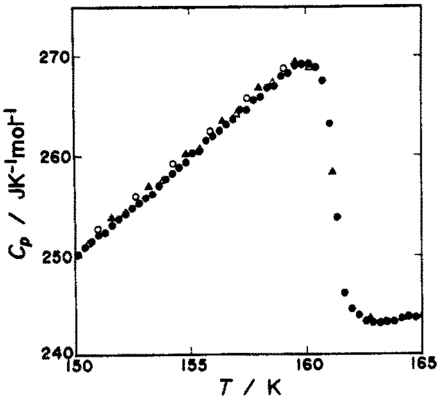

Fig. 2. Heat capacity of $(ND_4DC_2O_4)_2 \cdot D_2O$ in the vicinity of the phase transition. (○), Series 1 (cooled down to 79.79 K); (●), series 2 (148.82 K); (△), series 10 (146.45 K); (▲), series 12 (115.01 K). The data in series 10 and 12 are not included in Table 3.

Of the 81 degrees of freedom in AHO or ADO, 57 could be determined from the vibrational analyses as enumerated in Table 1. They were used in the calculation of the known part of the normal heat capacity.

There are 24 vibrational degrees of freedom whose frequencies could not be determined spectroscopically. These frequencies were determined from the heat capacity data by minimizing the following function using a non-linear least-squares method on a microcomputer:

$$F(\theta_D, \theta_{E,j}, A) = \sum_i [C_p(T_i) - AT_i\{C_p(T_i)\}^2 - C_v(\text{calc}) - C_v(\text{fitted})]^2.$$

Here C_v(calc) are the harmonic oscillator heat capacities summed over the 57 known modes;

$$C_v(\text{fitted}) = 6RD(\theta_D/T_i) + \sum_{j=1}^{3} n_j RE(\theta_{E,j}/T_i),$$

where R is the gas constant, $D(\theta_D/T_i)$ the Debye function with the characteristic temperature θ_D at $T = T_i$, $E(\theta_{E,j}/T_i)$ the Einstein function with the characteristic temperature $\theta_{E,j}$ at $T = T_i$ and n_j the weight (accidental degeneracy, because none is expected from the symmetry); and $AT_i\{C_p(T_i)\}^2$ is the

Table 4. Optimized parameters of the normal heat capacity functions

	$(NH_4HC_2O_4)_2\cdot H_2O$		$(ND_4DC_2O_4)_2\cdot D_2O$	
Temperature range (number) of points used for the fitting				
	13.35–39.40 K	(29)	13.95–66.29 K	(26)
	175.96–300.83 K	(19)	207.42–299.27 K	(19)
Parameter		Degen.		Degen.
θ_D (K)	141.5 ± 0.2	6	133.8 ± 0.3	6
θ_{E1} (K)	191.0 ± 0.3	8	181.8 ± 0.8	7
θ_{E2} (K)	367.5 ± 2.0	6	287.8 ± 1.3	7
θ_{E3} (K)	891.4 ± 6.9	4	698.2 ± 3.4	4
$A \times 10^7$ (mol·J^{-1})	8.60 ± 0.04		7.05 ± 0.03	

$C_p - C_v$ correction term. The last term may be written as $AT_t\{C_v(\text{calc}) + C_v\ (\text{fitted})\}^2$, which is formally more satisfactory, with a slight change of the meaning of A. The present form was used because of the simplicity of the calculation.

Results of the fitting are summarized in Table 4, and shown graphically by the dotted lines in Fig. 1. The excess heat capacities of AHO and ADO are plotted in Figs 3 and 4, respectively.

The excess heat capacities were integrated to obtain the molar enthalpy and entropy of the transition. The thermodynamic quantities associated with the transition are given in Table 5. The transition entropies (especially that of AHO) are close to $R\ln 2$ ($= 5.763$ J K^{-1} mol^{-1}). Since the mole as defined here contains two moles of ammonium ion, the experimental transition entropies indicate that only one of the two ammonium ions is disordered in the high temperature phase. This agrees with the crystal structure presented in Ref. 1 whose Fig. 6 shows a double peak distribution of hydrogen H(4) belonging to one of the ammonium ions.

If the statistical character of the disordered ammonium ion is the same in the deuterated compound, one should expect the same transition entropy ($\simeq R\ln 2$) for ADO. However, the actual transition entropy of ADO was larger than for AHO. This may simply indicate that the harmonic oscillator approximation is inadequate for the deuterate, which is probable because there are more energy levels related to the rotational motion of the ND_4^+ ion than the NH_4^+ ion in view of the low barrier height (~ 230 K [6]). The heat capacity of the hindered rotation of the ND_4^+ ion may be significantly larger than that given by the harmonic approximation. According to this view, a more elaborate evaluation of the base line of the heat capacity would eliminate the discrepancy between the transition entropies of the normal and deuterated compounds.

Another possible explanation of the H–D difference is to assume different mechanisms for them. As Fig. 5 shows, the excess heat capacities have different temperature dependences below as well as above T_{trs}. Most of the difference in the transition entropies comes from the difference of the excess heat capacities at low temperature. The difference increases approximately linearly from zero to *ca* 5 J K^{-1} mol^{-1} as the temperature increases from *ca* 0.5 T_{trs} to T_{trs}, then decreases gradually and is strongly temperature-dependent above T_{trs}. The larger excess heat capacity of the deuterate sample above T_{trs} indicates a more significant short range order effect in this compound. Since such a difference in the excess heat capacities does not seem to be removed simply by re-evaluating the base line, one may have to invoke a different mechanism, such as strong coupling between the hindered rotation and the microscopic order parameter, to explain the H–D difference of the transition entropies.

3.3. *Application of the Ehrenfest equation*

The temperature dependence of the lattice parameters of AHO [4] gives $V\Delta\alpha = (\partial V_H/\partial T)_p - (\partial V_L/\partial T)_p$, where V is the molar volume, $\Delta\alpha$ the change of the

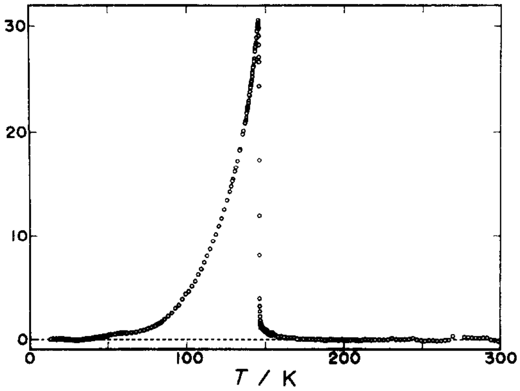

Fig. 3. Excess heat capacity of $(NH_4HC_2O_4)_2\cdot H_2O$.

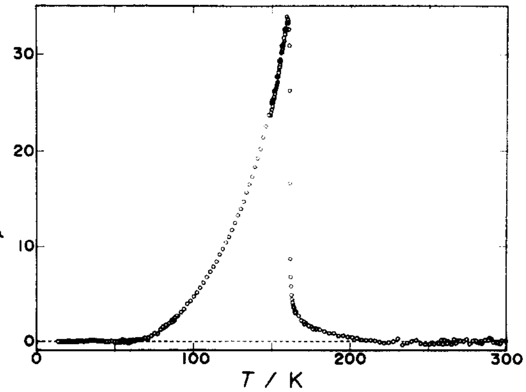

Fig. 4. Excess heat capacity of $(ND_4DC_2O_4)_2\cdot D_2O$.

Table 5. Thermodynamic quantities of the phase transition in $(NH_4HC_2O_4)_2 \cdot H_2O$ and $(ND_4DC_2O_4)_2 \cdot D_2O$

	T_{trs} (K)	$\Delta_{trs}H$ ($kJ \cdot mol^{-1}$)	$\Delta_{trs}S$ ($J \cdot K^{-1} \cdot mol^{-1}$)
$(NH_4HC_2O_4)_2 \cdot H_2O$	145.4	0.73	6.01
$(ND_4DC_2O_4)_2 \cdot D_2O$	160.1	1.11	8.23

thermal expansion coefficient at the transition temperature, and V_H and V_L are the molar volume of the high and low temperature phases, respectively. The $V\Delta\alpha$ value was read from Fig. 3(d) of Ref. 4,

$$\begin{aligned} V\Delta\alpha &= (\partial V_H/\partial T)_p - (\partial V_L/\partial T)_p \\ &= (0.1128 - 0.042) \times 10^{-30} \\ &\quad \times 6.022 \times 10^{23}/4 \\ &= 1.066 \times 10^{-8}\,m^3\,K^{-1}\,mol^{-1}. \end{aligned}$$

In Ref. 4, the unit cell contains eight $NH_4HC_2O_4 \cdot 1/2H_2O$ molecules. But we regard $(NH_4HC_2O_4)_2 \cdot H_2O$ as one mole, i.e. four molecules are involved in the unit cell described in Ref. 4. The factor 1/4 changes the volume per unit cell in Ref. 4 to our molar volume.

The change of the molar heat capacity at the phase transition, $\Delta_L^H C_p$ ($= C_p(\text{HTP}) - C_p(\text{LTP})$), is determined in the present experiment:

$$\Delta_L^H C_p = -30.6\,J\,K^{-1}\,mol^{-1}.$$

Substitution into the Ehrenfest equation leads to

$$\begin{aligned} \frac{dP}{dT} = \frac{\Delta_L^H C_p}{TV\Delta\alpha} &= \frac{-30.6}{145.38 \times 1.066 \times 10^{-8}} \\ &= -1.97 \times 10^7\,Pa\,K^{-1}. \end{aligned}$$

This agrees excellently with the actual slope of $dP/dT = -1.9 \times 10^7\,Pa\,K^{-1}$ of the transition line read off from the phase diagram [6, 7]. A similar comparison for ADO has not been made, because its volumetric data are not available.

3.4. *Calculation of the standard thermodynamic functions*

The standard thermodynamic functions of AHO and ADO are tabulated in Tables 6 and 7, respectively. The experimental heat capacities of AHO between 13.4 and 103.3 K, 90.5 and 145.4 K and 147.8 and 300.8 K were fitted by 10th-, 12th- and 12th-order polynomials, respectively. For ADO, the heat capacity data were divided into three temperature regions, i.e. 13.9–133.8 K, 120.8–160.1 K and

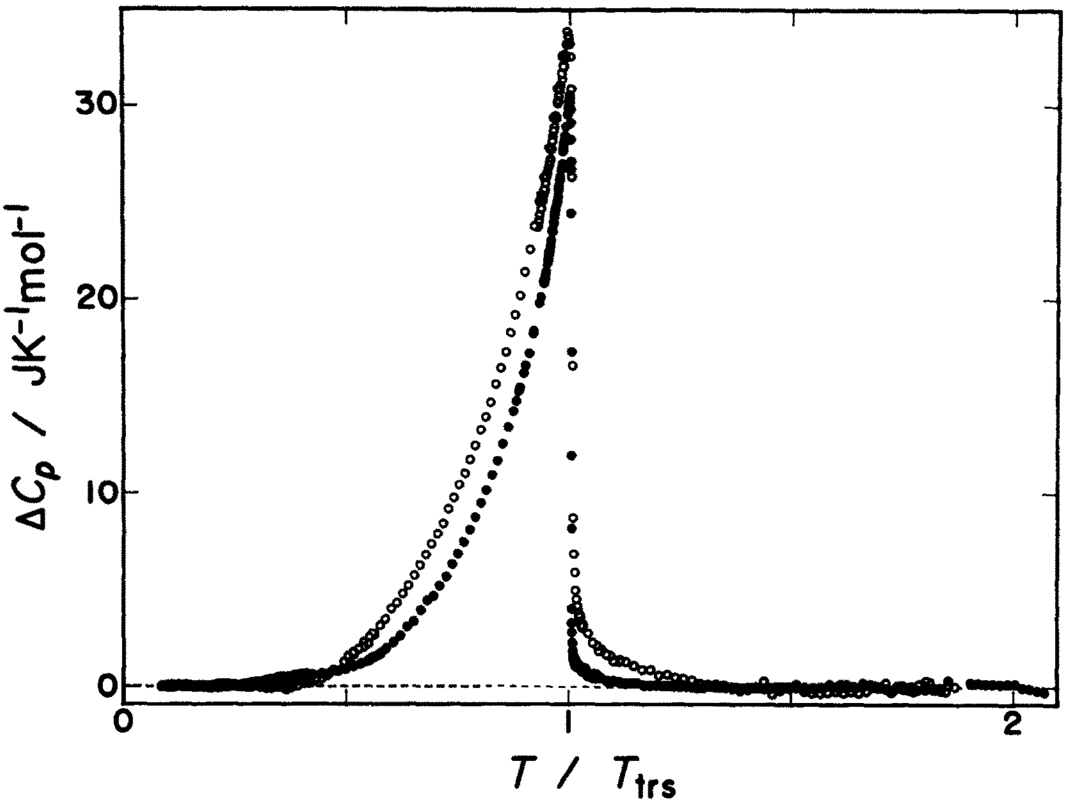

Fig. 5. Temperature dependence of the excess heat capacities of $(NH_4HC_2O_4)_2 \cdot H_2O$ and $(ND_4DC_2O_4)_2 \cdot D_2O$ plotted against the reduced temperature. (●), $(NH_4HC_2O_4)_2 \cdot H_2O$ (AHO); (○), $(ND_4DC_2O_4)_2 \cdot D_2O$ (ADO).

Table 6. Standard thermodynamic functions of $(NH_4HC_2O_4)_2\cdot H_2O$

$\frac{T}{K}$	$\frac{C^\circ_p}{R}$	$\frac{H^\circ(T)-H^\circ(0)}{RT}$	$\frac{S^\circ(T)-S^\circ(0)}{R}$	$-\frac{[G^\circ(T)-H^\circ(0)]}{RT}$
0	0	0	0	0
5†	0.02063	0.005159	0.006882	0.001722
10†	0.1675	0.04148	0.05526	0.01378
15†	0.5940	0.1447	0.1919	0.04719
20†	1.381	0.3484	0.4625	0.1141
25†	2.448	0.6580	0.8812	0.2232
30†	3.676	1.057	1.434	0.3773
35†	4.970	1.523	2.098	0.5745
40	6.282	2.036	2.847	0.8110
45	7.573	2.580	3.662	1.082
50	8.823	3.142	4.525	1.383
60	11.17	4.288	6.344	2.057
70	13.32	5.427	8.230	2.804
80	15.32	6.540	10.14	3.601
90	17.23	7.622	12.06	4.434
100	19.09	8.677	13.97	5.292
110	20.90	9.705	15.87	6.167
120	22.75	10.71	17.77	7.055
130	24.68	11.71	19.67	7.952
140	26.87	12.72	21.57	8.857
		Phase transition at 145.4 K		
150	25.35	13.65	23.42	9.768
160	26.45	14.41	25.09	10.67
170	27.55	15.15	26.72	11.57
180	28.63	15.87	28.33	12.46
190	29.70	16.57	29.91	13.33
200	30.73	17.26	31.46	14.20
210	31.74	17.92	32.98	15.06
220	32.74	18.57	34.48	15.91
230	33.73	19.21	35.96	16.75
240	34.69	19.83	37.41	17.58
250	35.64	20.45	38.85	18.40
260	36.58	21.05	40.26	19.21
270	37.54	21.64	41.66	20.02
273.15	37.85	21.83	42.10	20.27
280	38.50	22.23	43.05	20.82
290	39.41	22.81	44.41	21.61
298.15	40.15	23.27	45.52	22.25
300	40.31	23.37	45.76	22.39

† Quantities represent heat capacities extrapolated or interpolated by using the normal heat capacity function (combination of the Debye and Einstein functions), and other thermodynamic functions derived from them.

163.8–299.3 K, and fitted separately by 12th-order polynomials. The standard thermodynamic functions were calculated by the use of these polynomials. Quantities close to the transition region were evaluated by numerical integration, and added to the values from the polynomial contribution.

4. CONCLUSION

Calorimetric experiments showed the occurrence of gradual phase transitions in AHO and ADO crystals. The excess heat capacities are significant already at 1/2 T_{trs}. Determination of the transition entropies of such broad phase transitions is often hampered by the arbitrariness involved in the subtraction of the phonon contribution from the experimental heat capacity. This was minimized in the present case by the use of vibrational spectroscopic data and by the non-linear least-squares procedure. The results of the heat capacity analyses showed that one of the two non-equivalent ammonium ions is disordered in the high temperature phase. For ADO, however, the transition entropy was found to be larger than was predicted by a simple two-fold orientational disorder of the ND_4^+ ion. It is not clear whether or not this indicates a change in the mechanism of the phase transition on deuteration.

The anomalous heat capacity remains finite at the transition temperature, $\Delta C_p = 30.6\ \mathrm{J\,K^{-1}\,mol^{-1}}$ for the normal compound and $33.9\ \mathrm{J\,K^{-1}\,mol^{-1}}$ for the deuterate. For the hydrogenous compound, the gap

Table 7. Standard thermodynamic functions of $(ND_4DC_2O_4)_2\cdot D_2O$

T	C_p°	$H^\circ(T)-H^\circ(0)$	$S^\circ(T)-S^\circ(0)$	$-[G^\circ(T)-H^\circ(0)]$
K	R	RT	R	RT
0	0	0	0	0
5 †	0.02439	0.006099	0.008135	0.002036
10 †	0.1973	0.04897	0.06526	0.01628
15 †	0.6838	0.1688	0.2243	0.05551
20 †	1.546	0.3982	0.5310	0.1327
25 †	2.681	0.7378	0.9940	0.2562
30	3.973	1.168	1.596	0.4275
35	5.334	1.665	2.310	0.6442
40	6.711	2.210	3.112	0.9017
45	8.074	2.786	3.981	1.195
50	9.405	3.382	4.901	1.519
60	11.94	4.599	6.843	2.243
70	14.28	5.817	8.861	3.044
80	16.46	7.012	10.91	3.899
90	18.51	8.177	12.97	4.792
100	20.47	9.308	15.02	5.713
110	22.36	10.41	17.06	6.652
120	24.23	11.48	19.09	7.604
130	26.10	12.54	21.10	8.565
140	28.05	13.57	23.11	9.532
150	30.10	14.61	25.11	10.50
160	32.38	15.65	27.13	11.48
Phase transition at 160.1 K				
170	29.84	16.48	28.94	12.46
180	30.91	17.26	30.68	13.42
190	32.01	18.00	32.38	14.37
200	33.09	18.73	34.05	15.32
210	34.15	19.44	35.69	16.25
220	35.21	20.13	37.30	17.17
230	36.28	20.81	38.89	18.08
240	37.32	21.48	40.45	18.98
250	38.35	22.13	42.00	19.87
260	39.40	22.77	43.52	20.75
270	40.43	23.41	45.03	21.62
273.15	40.75	23.61	45.50	21.89
280	41.45	24.04	46.52	22.48
290	42.48	24.65	47.99	23.34
298.15	43.29	25.15	49.18	24.03
300	43.51	25.27	49.45	24.18

† Quantities represent heat capacities extrapolated or interpolated by using the normal heat capacity function (combination of the Debye and Einstein functions), and other thermodynamic functions derived from them.

is consistent with the Ehrenfest relationship for the second-order phase transitions at the phenomenological level of the discussion. From the model theoretical point of view, they are much larger than the 3/2 R predicted by the molecular field approximation, and probably indicate the significance of the fluctuation of the order parameter near T_{trs}.

REFERENCES

1. Küppers H., *Acta crystallogr.* **B29**, 318 (1973).
2. Küppers H., *Acta crystallogr.* **A28**, 522 (1972).
3. Küppers H., *Z. Kristallogr.* **140**, 393 (1974).
4. Keller H. L., Kucharczyk D. and Küppers H., *Z. Kristallogr.* **158**, 221 (1982).
5. Benoit J. P., Berger J., Krauzman M. and Godet J. L., *J. Phys. (Paris)* **47**, 815 (1986).
6. Godet J. L., Krauzman M., Mathieu J. P., Poulet H. and Toupry N., *J. Phys. (Paris)* **48**, 809 (1987).
7. Krauzman M., Godet J. L., Pick R. M., Poulet H., Toupry N., Bosio L., Debeau M., Launois P. and Moussa F., *Europhys. Lett.* **6**, 37 (1988).
8. Tatsumi M., Matsuo T., Suga H. and Seki S., *Bull. chem. Soc. Japan* **48**, 3060 (1975).
9. Matsuo T. and Suga H., *Thermochim. Acta* **88**, 149 (1985).
10. Villepin J. and Novak A., *Spectrochim. Acta* **27A**, 1259 (1971).